Journal of the Korean Society for Nondestructive Testing
Vol. 28, No. 3 (2008. 6)

Reflection and Transmission of Acoustic Waves Across Contact Interfaces

Nohyu Kim*†, Kyung-Young Jhang**, Taehoon Lee***, Seungyong Yang****
and Youngchul Chang*

Abstract A linearized model for hysteretic acoustic nonlinearity of imperfectly joined interface is proposed and analyzed by using Coulomb damping to investigate the characteristics of the reflection and transmission coefficients for harmonic waves at the contact interface. Closed crack is modeled as non welded interface that has nonlinear discontinuity condition in displacement across its boundary. Based on the hysteretic contact stiffness of the contact interface, the reflected and transmitted waves are determined by deriving the tractions on both sides of the interface in terms of the discontinuous displacements across the interface. It is found that the amplitudes of the reflected and transmitted waves are dependent on the frequency and the hysteretic stiffness. As the frequency of the incident wave increases, the higher reflection and lower transmission are obtained. It also shows that the hysteresis of the interface increases the reflection coefficient, but reduces the transmission coefficient. A fatigue crack is also made in aluminum specimen to demonstrate these characteristics of the reflection and transmission of contact interfaces.

Keywords: Reflection/Transmission Coefficients, Contact Nonlinearity, Hysteresis, Closed Crack

1. Introduction

Contact-type discontinuity such as closed cracks leads to an anomalously high level of nonlinearity. Well-known acoustical manifestation of the nonlinear behavior is the generation of its harmonics. The practical implementation of the second harmonic method has been widely attempted to assess the contact state or to detect a cracks in NDE applications. In particular, the transmission and reflection characteristics at contacting surfaces have been the subject of extensive research relating to the evaluation of contact interfaces and integrity monitoring in NDT. The physical nature of the contact acoustic nonlinearity(CAN) has been explained and analyzed by a micro-mechanical models for contact-type interface. The variation of contact area due to the deformation of asperities is known to cause the nonlinear elasticity of interfaces. In the previous works, this interface is considered as a nonlinear elastic spring whose stiffness is proportional to the contact area of interfaces (Biwa et al., 2006 and 2007; Delsanto et al., 2002; Kim et al., 2004).

However, the CAN reveals not only the nonlinear elastic behavior, but also a hysteretic deformation during loading and unloading cycles

Received: May 8, 2007, Revised: June 16, 2008, Accepted: June 19, 2008 * Department of Mechatronic Engineering, Korea University of Technology and Education, Chunan 330-860, Korea ** Department of Mechanical Engineering, Hanyang University, Seoul 133-791, Korea *** Graduate School of Mechanical Engineering, Hanyang University, Seoul 133-791, Korea **** Department of Mechanical Engineering, Korea University of Technology and Education, Chunan 330-860, Korea † Corresponding author: nykim@kut.ac.kr

(Biwa, 2007; Kim, 2006). With respect to the physical micro-mechanism of hysteresis, there are two major explanations. The first explanation consisted in hysteretic frictional sliding between grain contacts and solid boundaries (Zumpano and Meo, 2007). For nearly 30 years, hysteretic friction was believed to be the dominant mechanism until 1994, when a certain discrepancies of the traditional approach at high ambient pressure were reported. The alternative explanation is adhesion hysteresis, which accounts for hysteresis and losses even if the contacts are strongly compressed and no intergranular friction is possible. The adhesion hysteresis exists when the strain energy release rate required for growth of the contact area during loading is much lower than that required for the decrease in contact area during unloading. This difference may arise from a bulk visco-elasticity, or from a mechanical change of the materials at their interface. The explanation was, however, only qualitative, and the quantitative theory that predicts the shape of the stress–strain hysteresis from statistical data on the micro-geometry was not built. Besides the adhesion and friction hysteresis, several other physical mechanisms may also contribute to the hysteretic constitutive behavior of materials with internal contacts. They include the stick–slip motion of asperities, and the movement of dislocations (Nazarov and coworkers in 2003). In addition, Kim et al. (2006) demonstrated that hysteresis in the stress–strain relation may follow directly from the elasto-plastic loading and elastic unloading of a rough contact. A more practical approach to dealing with hysteresis and its effects is the application of the Preisach–Mayergoyz (PM) space to the problem of nonlinear elasticity. The approach using two-state relays for "open" and "closed" cracks has been adapted to the researches on the hysteretic acoustical nonlinearity in damaged materials (Aleshin and Van Den Abeele, 2007).

In this paper both friction and adhesion approaches for hysteresis are combined to build a new stress–strain constitutive equation based on a displacement discontinuity analysis. Subsequently this relation is applied to simulate the reflection and transmission of a harmonic wave across the contact interface using an analogous formulation of wave equation. Theoretically, the transmission/ reflection spectra of the normally incident longitudinal and shear waves are governed by the normal and tangential stiffnesses of contact interfaces (Biwa, 2005). These interfacial stiffnesses offer useful information on the nature of the contact interface, and especially for the detection of a closed crack that does not produce linear scattering waves. For these reasons, a parametric study is conducted to investigate the effects of interfacial properties such as the interface stiffness and hysteresis on the reflection and transmission of acoustic waves. In addition, a fatigue crack is made in aluminum plate and is scanned by 5 MHz transducer of 0.25 inch diameter to measure the reflection and transmission waves across the crack at various locations. The experimental results are compared with the theoretical results, and discussed to evaluate the model proposed in this paper.

2. Hysteretic Nonlinear Displacement Discontinuity Model for Contact Interface

Closed cracks in solid medium represent a mechanical discontinuity that strongly affects the propagation of elastic waves either across or along the crack boundary. At the micro-scale, the contact interface appears as two surfaces of irregular topology which intersect to form micro-void spaces and asperities of contact. The presence of the asperities and voids within a planar crack define a thin, compliant zone with effective normal and shear stiffnesses that can range from near zero for open crack to almost infinite values for completely closed crack which are bonded or subjected to high compressive stresses. Typically a crack loaded in shear or compression exhibits a highly nonlinear stress-

displacement relationship resulting from plastic deformation of the asperities. The hysteresis is also accompanied with the classical nonlinear elasticity as shown in the stress-displacement curve in Fig. 1(a) during loading and unloading, indicating the presence of inelastic deformation of the asperities of contact and frictional sliding between contacts(Kim et al, 2004 and 2006). Those features of closed cracks play an important role in the interaction with elastic waves. The interface stiffness is the quantity that relates the displacement to the traction of closed contact interfaces, which may be linear or nonlinear. In linear displacement discontinuity model or imperfect interface model (Pyrak-Nolte et al., 1990), two contact surfaces of each boundary are assumed to be continuous in stress but not in displacement at which the specific stiffness is defined as a linear spring such that the stress is proportional to the displacement difference.

Let us consider a nonlinear hysteretic-oscillatory cycle $S_L - S_U$ between two

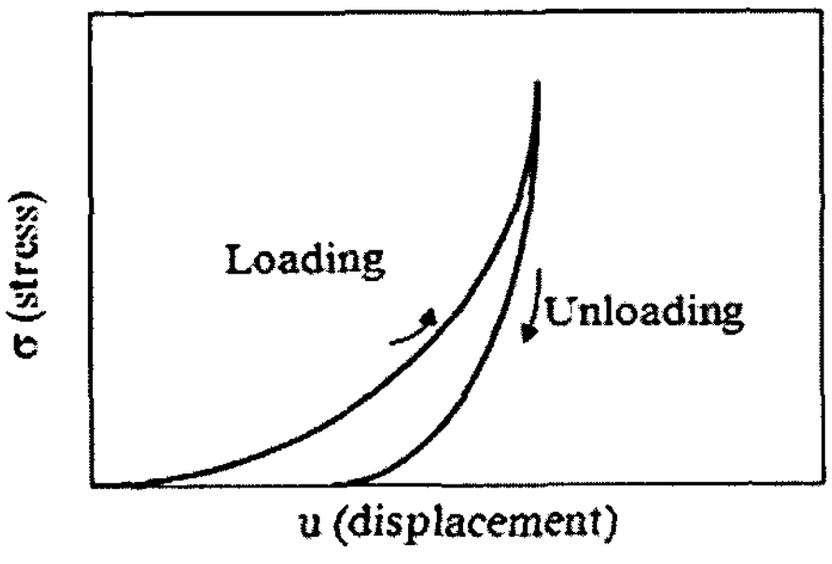

Fig. 1 Hysteretic behavior of contact interfaces (a) loading unloading curves, (b) idealized hysteresis

deformation states, u_1 and u_2, in Fig. 1(b) caused by acoustic waves. The irreversible deformation starts from u_1 to u_2 following a loading path S_L and returns to the original point u_1 via an unloading path S_L completing one cycle of motion. A linear deformation path S from u_1 to u_2 is also presented in Fig. 1(b) to introduce the linear stiffness κ from the proportional linearity. During the loading process S_L of this hysteresis cycle, the work done to the medium by stress is larger than that of the linear loading S, while the work done during the unloading process S_U is smaller than that of the linear unloading. The amount of the energy difference is dissipated by the hysteresis of contact interfaces. In these processes, the contact interface works as a non-classical hysteretic spring that gets stiffer during loading and softer for unloading. Thus this characteristic of the hysteretic spring can be formulated by adding a supplementary stiffness to the linear spring during loading, and subtracting the same stiffness from the linear spring during unloading (Kim and Yang, 2007). Such a hysteretic spring force can be considered as Coulomb friction force and/or viscous force. In this paper, a hysteretic nonlinear stiffness κ_n is defined such that the hysteretic force is linearly proportional to the displacement history $\Delta u = (u_2 - u_1)$. The hysteretic nonlinear stiffness κ_n is complex and can be determined by calculating the energy loss dissipated by one cycle of the process $S_U - S_L$. Based on these assumptions, the stress-displacement relation across the interface in the process $S_U - S_L$ is linearized and expressed by the superposition of a linear spring κ and nonlinear hysteretic spring κ_n as follows.

$$\begin{aligned}
&\sigma(u_1 + \Delta u) = P + \kappa \cdot (\Delta u) + \kappa_n \cdot (\Delta u) \\
&\quad for\ loading(S_L): \Delta u = u_2 - u_1 > 0 \\
&\sigma(u_1 + \Delta u) = P + \kappa \cdot (\Delta u) - \kappa_n \cdot (\Delta u) \\
&\quad for\ unloading(S_U): \Delta u = u_2 - u_1 < 0 \\
&P = \sigma(u_1): \ pressure\ in\ equillibrium
\end{aligned} \tag{1}$$

Now suppose that two elastic bodies with identical material properties are put into contact by static pressure P. Due to the surface roughness, the contact at the interface forms a microscopically imperfect elastic-plastic deformation between the upper (denoted by superscript u) and lower (denoted by superscript l) rough surfaces as shown in Fig. 2(a). The displacement vectors of the upper and lower surface are given in Fig. 2(a) by $\boldsymbol{u}^u = (u_x^u, u_z^u)$ and $\boldsymbol{u}^l = (u_x^l, u_z^l)$. The sizes of asperities are assumed to be much smaller than the wavelength of acoustic wave so that the incoherent scattering from the interface is negligible. Since both the displacement and the stress have discontinuity across the interface, some boundary conditions are necessary to connect those discontinuities. These conditions are obtained from the constitutive properties of the interface formulated by the hysteretic nonlinear spring κ_n in eqn. (1). Those provide the relationship between the tractions and the displacement across and along the interface in normal and shear directions (z and x in Fig. 2). To do so, applying the stress-displacement relations in eqn. (1) to the contact interfaces in Fig. 2 yields the following constitutive equations.

$$
\begin{aligned}
\boldsymbol{t}_x^u &= P + \kappa_x(\Delta u_x) + \kappa_{nx}(\Delta u_x) = \\
&\quad P + \kappa_x(u_x^u - u_x^l) + \kappa_{nx}(u_x^u - u_x^l) \\
\boldsymbol{t}_x^l &= P + \kappa_x(\Delta u_x) - \kappa_{nx}(\Delta u_x) = \\
&\quad P + \kappa_x(u_x^u - u_x^l) - \kappa_{nx}(u_x^u - u_x^l) \\
\boldsymbol{t}_z^u &= P + \kappa_z(\Delta u_z) + \kappa_{nz}(\Delta u_z) = \\
&\quad P + \kappa_z(u_z^u - u_z^l) + \kappa_{nz}(u_z^u - u_z^l) \\
\boldsymbol{t}_z^l &= P + \kappa_z(\Delta u_z) - \kappa_{nz}(\Delta u_z) = \\
&\quad P + \kappa_z(u_z^u - u_z^l) - \kappa_{nz}(u_z^u - u_z^l)
\end{aligned}
\tag{2}
$$

In eqn. (2), $\boldsymbol{t}_x^u, \boldsymbol{t}_x^l, \boldsymbol{t}_z^u, \boldsymbol{t}_z^l$ are the shear and normal tractions on the upper and lower surfaces, κ_x and κ_z are the linear normal and shear stiffnesses, κ_{nx} and κ_{nz} the hysteretic nonlinear normal and shear stiffnesses, and $u_x^u, u_x^l, u_z^u, u_z^l$ are the displacements of the upper and lower surfaces in x and z as shown in Fig. 2(a). The sign of the hysteretic nonlinear stiffness in eqn. (2) stands for the loading and unloading states of the lower and upper boundary surfaces in Fig. 2. A positive sign is assigned to the stiffnesses κ_{nx} and κ_{nz} if the relative displacement of the boundaries increases with the coordinate x and z, and a negative sign is assigned if the relative displacement decreases with the coordinate x and z. It is clear from this sign rule that the tractions on the lower surface of Fig. 2 work as if they provoke an unloading process of the hysteresis defined in Fig. 1. It is also observed from eqn. (2) that if the hysteretic nonlinear stiffnesses, κ_{nx} and κ_{nz}, are all zero, eqn. (2) gives $\boldsymbol{t}_x^u = \boldsymbol{t}_x^l$, $\boldsymbol{t}_z^u = \boldsymbol{t}_z^l$, which means a stress continuity across the interface. This stress continuity at the interface is the boundary conditions of the classical nonlinear contact models (Pyrak-Nolte et al., 1990). Eqn. (2) also represents the limiting cases for a traction-free

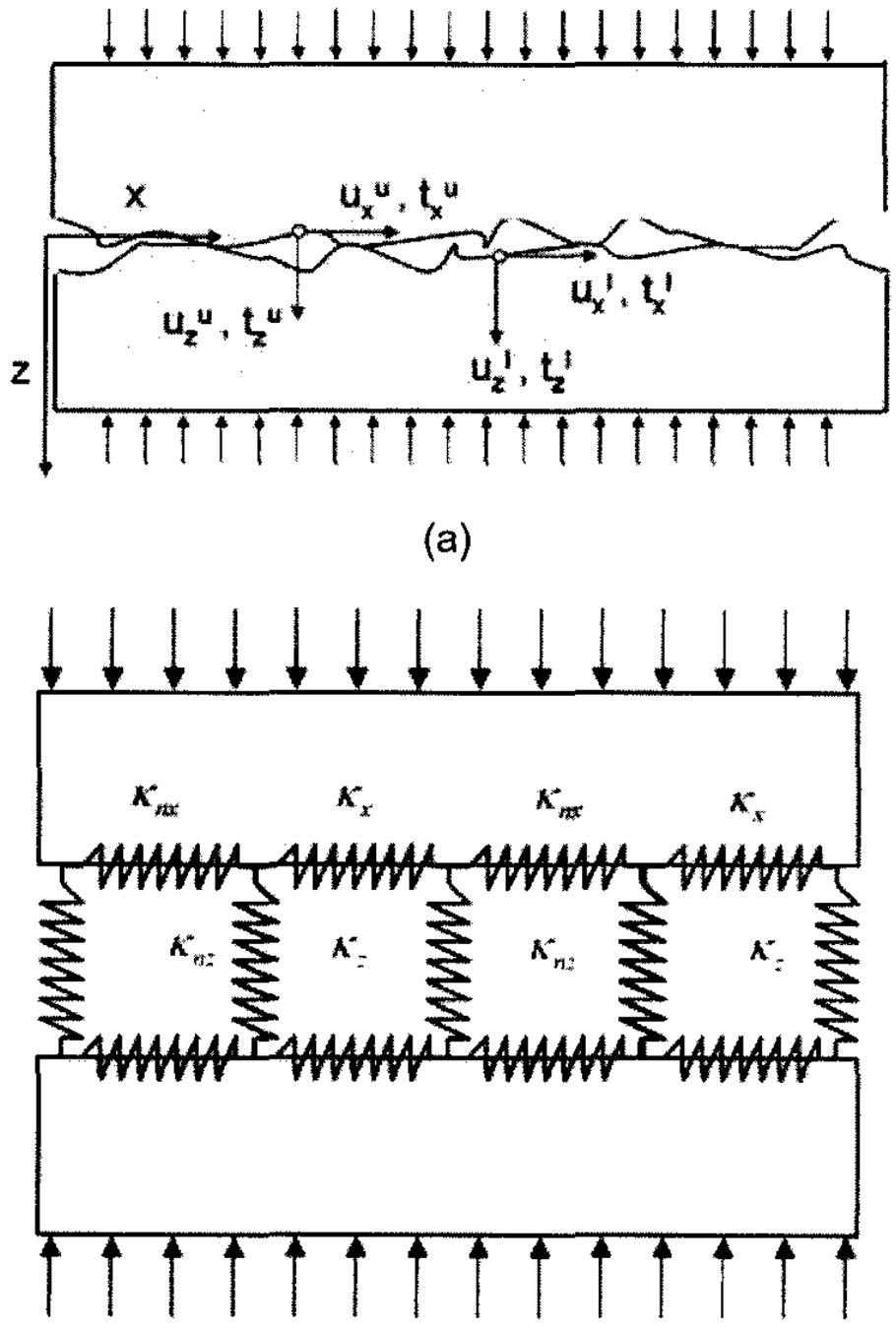

Fig. 2 Contacting rough surfaces; (a) the tractions and displacements of boundaries, (b) mathematical spring model

boundary condition as κ_x and κ_z go to zero, and for a welded interface as κ_x and κ_z become infinity. Eqns. (1) and (2) describe a simple but pertinent constitutive model for the hysteretic nonlinear behavior of a non-welded contact between two identical media.

3. Transmission and Reflection of Harmonic Waves at Interface

The reflection and transmission of acoustic waves across contact interface have been investigated and understood well using the classical nonlinear spring model of contact interface (Biwa et al., 2005; Kim et al., 2006; Solodov, 1998). For the analysis of the reflection/transmission characteristics, a second-order Taylor approximation of general nonlinear stress-displacement relationship is used in the classical acoustic nonlinearity of a compressed contact interface. However, experimental evidences (Aleshin and Abeele, 2007; Zumpano and Meo, 2007) showed that classical nonlinear models cannot explain the non-classical nonlinear behavior generated by local nonlinear forces due to damage presence (such as cracks and contacts). Its explanation is possible by adding to the nonlinear classical stress–strain relationship, a stress dependence on strain time history. Due to the inadequacy of classical nonlinear material models to reproduce the behaviour of damaged materials, a new material constitutive model such as Presaich and Mayergoyz (PM) space, capable of accurately describing the nonlinear, discrete memory, and hysteretic behavior of such mate- rials, is introduced (Zumpano and Meo, 2007).

This hysteretic effect does not only play a key role in the pressure-strain relation and constitutive equation of a partly closed interface, but also contributes to the reflection and transmission of acoustic waves across the interface. In this work, a plane wave analysis is conducted by employing the hysteretic nonlinear displacement discontinuity model introduced in eqn. (2) of previous section to investigate the hysteretic effect of contact interfaces on the reflection and transmission coefficients of acoustic wave across the interface. Consider a longitudinal plane wave incident to the contact interfaces in z direction as shown in Fig. 3. Then the incident harmonic wave $\left(u_z^u(z,t)\right)_i = Ae^{ik(z-ct)}$ in the upper medium generates a reflected wave $\left(u_z^u(z,t)\right)_r = Be^{-ik(z+ct)}$ and a transmitted wave $\left(u_z^l(z,t)\right)_t = Ce^{ik(z-ct)}$ at the interface of Fig. 3. The amplitudes of the waves, A, B, and C, are a complex magnitude, and the superscripts, u and l , represent the upper and lower medium of the interface, and the subscripts, $r$and t, mean the reflection and transmission, respectively. From eqn. (2), the constitutive equations of the interface are given by

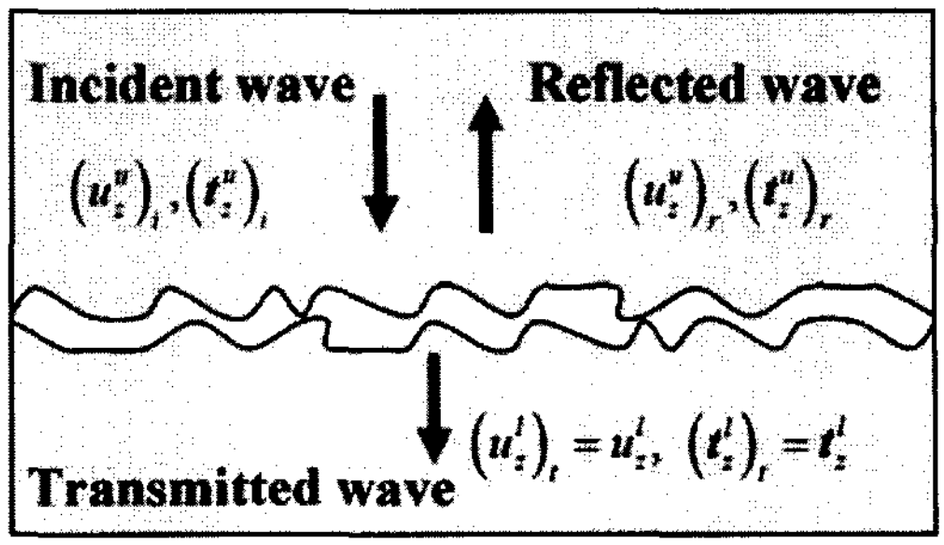

Fig. 3 Reflection and transmission of harmonic waves at contact interfaces

$$\begin{aligned} t_z^u + t_z^l &= 2\kappa_z(u_z^u - u_z^l) + 2P \\ t_z^u - t_z^l &= 2\kappa_{nz}(u_z^u - u_z^l) \end{aligned} \tag{3}$$

The tractions and displacements in eqn. (3) are decomposed into the tractions and displacements produced by the incident, reflected and transmitted waves as follows.

$$\begin{aligned} t_z^u &= \left(t_z^u\right)_i + \left(t_z^u\right)_r,\ t_z^l = \left(t_z^u\right)_t \\ u_z^u &= \left(u_z^u\right)_i + \left(u_z^u\right)_r,\ u_z^l = \left(u_z^l\right)_t \end{aligned} \tag{4}$$

Inserting eqn. (4) into eqn. (3), and differentiating it by the variable z produce the following differential equation.

$$\frac{\partial \boldsymbol{t}_z^u}{\partial z}+\frac{\partial \boldsymbol{t}_z^l}{\partial z}=2\kappa_z(\frac{\partial u_z^u}{\partial z}-\frac{\partial u_z^l}{\partial z})$$
$$\frac{\partial \boldsymbol{t}_z^u}{\partial z}-\frac{\partial \boldsymbol{t}_z^l}{\partial z}=2\kappa_{nz}(\frac{\partial u_z^u}{\partial z}-\frac{\partial u_z^l}{\partial z}) \quad (5)$$

From the wave equation,

$$\frac{\partial \mathbf{t}_z^u(z,t)}{\partial z}=\rho\frac{\partial^2 u_z^u(z,t)}{\partial t^2} \quad \text{and} \quad \frac{\partial \mathbf{t}_z^l(z,t)}{\partial z}=\rho\frac{\partial^2 u_z^l(z,t)}{\partial t^2} \quad (6)$$

$$\frac{\partial u_z^u(z,t)}{\partial z}=(\frac{1}{c})[\frac{\partial (u_z^u(z,t))_r}{\partial t}-\frac{\partial (u_z^u(z,t))_i}{\partial t}],$$
$$\frac{\partial u_z^l(z,t)}{\partial z}=(-\frac{1}{c})\frac{\partial (u_z^l(z,t))_t}{\partial t} \quad (7)$$

Substituting eqns. (6) and (7) into eqn. (5) yields the following differential equations for a new displacement $\delta(t)=u_z^u(0,t)-u_z^l(0,t)$,

$$\frac{\partial \delta(t)}{\partial t}-\alpha\delta(t)= 2(\alpha+i\omega)(u_z^u(0,t))_t-(2\alpha)(u_z^u(0,t))_i \quad (8)$$

$$\frac{\partial \delta(t)}{\partial t}-\beta\delta(t)= (2\beta)[(u_z^u(0,t))_t-(u_z^l(0,t))_i]$$

where, $\alpha=\frac{2\kappa_z}{\rho c_p}$, $\beta=\frac{2\kappa_{nz}}{\rho c_p}$, and C_p is the longitudinal wave velocities.

Eqn. (8) can be rearranged again in a simpler form,

$$\frac{\partial \delta(t)}{\partial t}-(\frac{i\omega\beta}{\alpha-\beta+i\omega})\delta(t)= -(\frac{2i\omega\beta}{\alpha-\beta+i\omega})(u_z^u(0,t))_i \quad (9)$$

Then the displacement $\delta(t)$ is obtained by solving eqn. (9) for the incident wave $(u_z^u(0,t))_i=Ae^{-i\omega t}$ as follows.

$$\delta(t)=\frac{2i\omega\beta}{i\omega\alpha-\omega^2}Ae^{-i\omega t} \quad (10)$$

Subsequently the reflected and transmitted waves can determined from eqn. (10) and be expressed in terms of dimensionless variables such as the velocity ratio of longitudinal wave to shear wave and specific stiffness as follows.

$$(u_z^l(z,t))_t=\frac{i\omega(\alpha-\beta)}{i\omega\alpha-\omega^2}Ae^{ik(z-ct)}= \frac{2i\frac{(\kappa_z-\kappa_{nz})}{Z_s\omega}}{2i(\frac{\kappa_z}{Z_s\omega})-(\frac{c_p}{c_s})}Ae^{ik(z-ct)}$$

$$(u_z^u(z,t))_r=\frac{i\omega\beta+\omega^2}{i\omega\alpha-\omega^2}Ae^{-ik(z+ct)}= \frac{2i(\frac{\kappa_{nz}}{Z_s\omega})+(\frac{c_p}{c_s})}{2i(\frac{\kappa_z}{Z_s\omega})-(\frac{c_p}{c_s})}Ae^{-ik(z+ct)} \quad (11)$$

$$(u_z^u(z,t))_i=Ae^{ik(z-ct)}$$

Therefore, the reflection and transmission coefficients at contact interfaces are simply given by

$$R(Reflection\ Coeff.)=\frac{(u_z^u(0,t))_r}{(u_z^u(0,t))_i}= \frac{2i(\frac{\kappa_{nz}}{Z_p\omega})+1}{2i(\frac{\kappa_z}{Z_p\omega})-1}$$
$$T(Transmission\ Coeff.)=\frac{(u_z^l(0,t))_t}{(u_z^u(0,t))_i}= \frac{2i\frac{(\kappa_z-\kappa_{nz})}{Z_p\omega}}{2i(\frac{\kappa_z}{Z_p\omega})-1} \quad (12)$$

In eqn. (12), $Z_p=\rho c_p$ is the acoustic impedances of the medium for longitudinal waves, and $\frac{\kappa_z}{\omega Z_p}, \frac{\kappa_{nz}}{\omega Z_p}$ are the specific linear and hysteretic stiffnesses, respectively. The reflection and transmission coefficients for the shear waves take the same form as that of the longitudinal waves in eqn. (12) except that κ_z and κ_{nz} are replaced by κ_x and κ_{nx}.

4. Parametric Study on Interface Characteristics

First of all, eqn. (12) explains two limiting boundary conditions for contact interfaces. One is the case that the interface is perfectly welded. In this case, the boundary disappears and the two solids behave like one continuous medium. Thus there is no reflection from the interface, and transmitted wave is equal to the incident wave. Since the linear stiffness κ_z of the interface is infinite for this case, the reflection coefficient of eqn. (12) becomes zero and the transmission coefficient unity. Therefore, it gives the same results as in a continuous solid medium. The other extreme case is that the interface is completely detached and separated each other (e.g., an open crack). When the interface loses contact, the stiffness of the interface goes to zero. Hence, the reflection coefficient is -1 from eqn. (12) and the transmission coefficient zero, which is same as for a free-end solid.

It is obvious from eqn. (12) that the dimensionless specific stiffnesses, $\frac{\kappa_z}{\omega Z_p}$ and $\frac{\kappa_{nz}}{\omega Z_p}$, are the key factors which determine the amplitude of the reflected and transmitted waves. Eqn. (12) also shows that the reflection and transmission of incident waves depend on acoustic wave frequency. The higher frequency the incident acoustic wave becomes, the higher reflection of acoustic waves is generated. Thus the interface is a good reflector for an ultrasound of high frequency, and becomes a bad reflector for a low frequency ultrasound. The variations of the reflection coefficient R due to the frequency change in amplitude and phase are presented in Fig. 4 when no hysteresis exists. Same figures for the transmission coefficient T are displayed in Fig. 5 for different values of hysteretic stiffness. In Figs. 4(a) and 5(a), the contact interface interacts with the incident wave differently depending on the frequency used. They show that contact interfaces act like a high -pass filter for reflection while it does like a low -pass filter for the transmission coefficient. This may be quite useful to detect a partly closed crack when using a short pulse of ultrasound instead of a tone-burst signal. If a crack is totally open, the reflection and transmission waves from the crack are independent of the frequency of incident wave. However, if it is partly closed, the magnitude of the reflection and transmission waves varies with the incident wave frequency. Therefore if an incident wave of wide bandwidth is applied to the interface, this selective characteristic of the reflected and transmitted waves can indicate a presence of a closed crack which cannot be found by traditional linear ultrasound. This fact agrees well with the experimental results reported by other studies (Biwa et al., 2006; Pyrak-Nolte, 1990).

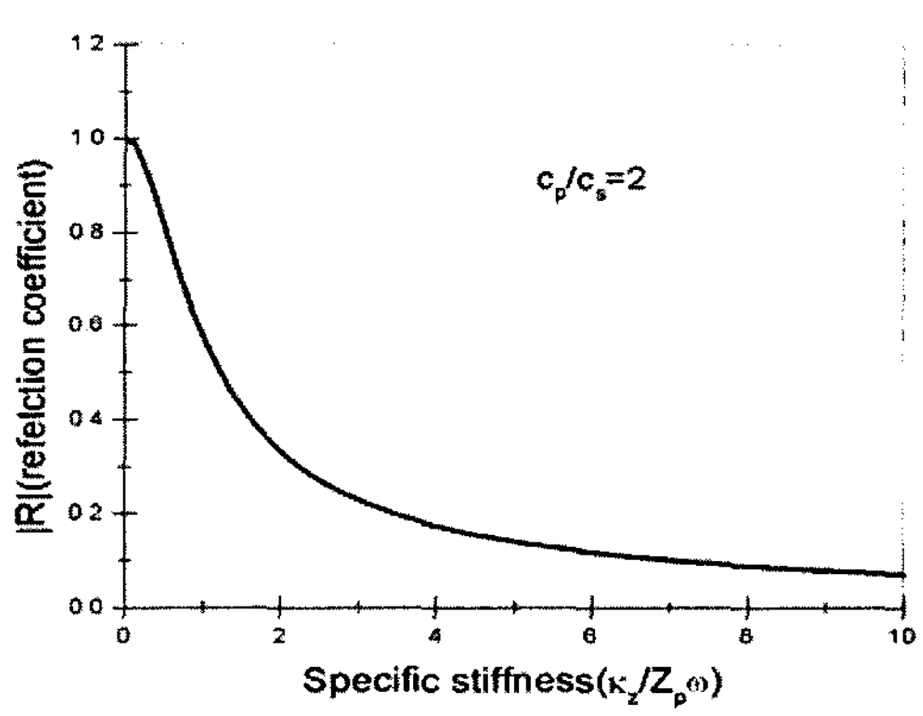

(a) the amplitude of R

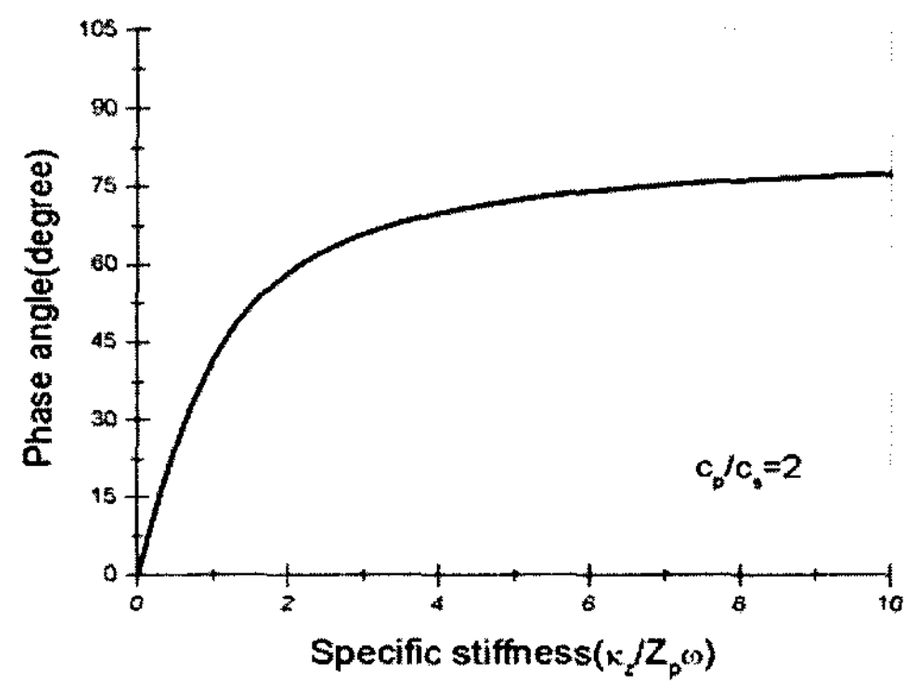

(b) the phase of R

Fig. 4 Reflection of reflected waves at contact interfaces with respect to the dimensionless specific stiffness $\frac{\kappa_z}{Z_p\omega}$

If all the specific stiffnesses, $\frac{\kappa_z}{\omega Z_p}$ and $\frac{\kappa_{nz}}{\omega Z_p}$, are much larger than unity or the frequency is very low, the asymptotes of the reflection and transmission coefficients are expressed by only an interface stiffness ratio; i.e., $R=\frac{\kappa_{nz}}{K_z}$, $T=1-\frac{\kappa_{nz}}{\kappa_z}$. This means that the hysteretic stiffness determines the reflection and transmission of the interfaces when a very low frequency is used. If the hysteretic nonlinear stiffness is negligible, eqn. (12) is reduced into

$$|R|=\frac{1}{\sqrt{1+4(\frac{\kappa_z}{Z_p\omega})^2}},\ phase=\tan^{-1}(2(\frac{\kappa_z}{Z_p\omega}))$$

$$|T|=\frac{2(\frac{\kappa_z}{Z_p\omega})}{\sqrt{1+4(\frac{\kappa_z}{Z_p\omega})^2}},\ phase=\tan^{-1}(\frac{1}{2(\frac{\kappa_z}{Z_p\omega})}) \quad (13)$$

Eqn. (13) is exactly same results reported from the classical nonlinear elasticity (Biwa et al., 2007).

5. Experimental Results

In order to demonstrate qualitatively the validity of the model proposed in this paper, a closed crack is created artificially using an EDM notch in aluminum 6061 plate. The aluminum specimen is 60×60 mm in size and 10 mm in thickness. A notch is made in the edge of the plate to initiate a crack in front of the notch by the accelerated fatigue test. The crack generated by low-cycle fatigue is shown schematically in Fig. 6, where it appears to propagate up to 10 mm from the tip of the notch. The crack seems to extend beyond 10 mm, but is not recognized surely by bare eyes because it is closed. The aluminum specimen with the crack is then examined by pulse-echo and through-transmission tests to measure the reflection and transmission energy across the crack using a tone-burst incident wave (5 MHz). Both the pulse -echo and transmission signals from the crack are

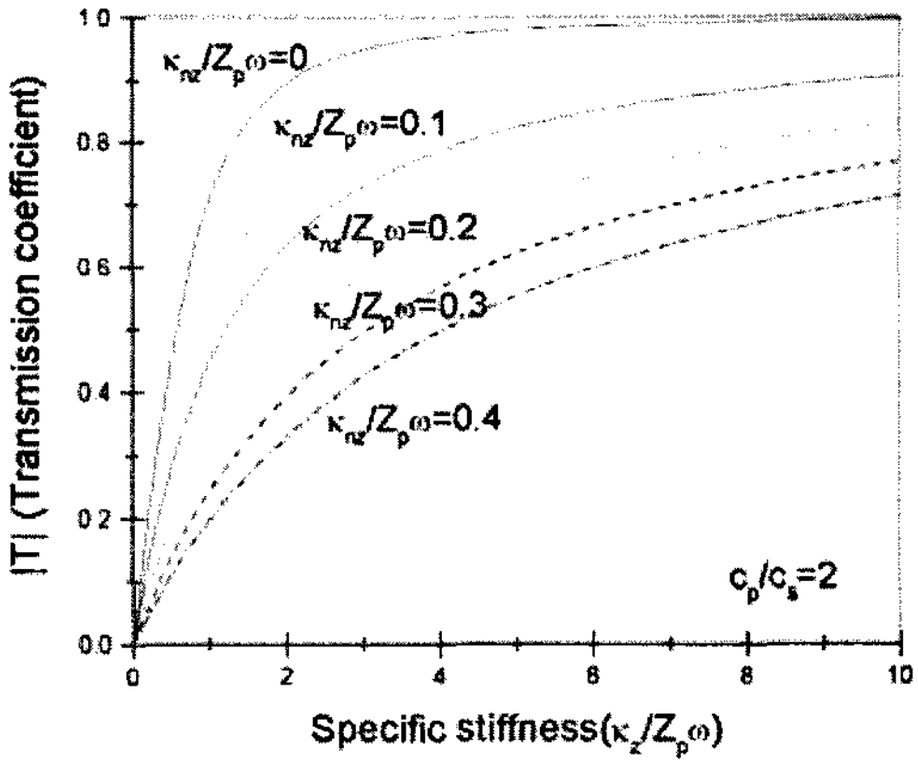

(a) the amplitude of T

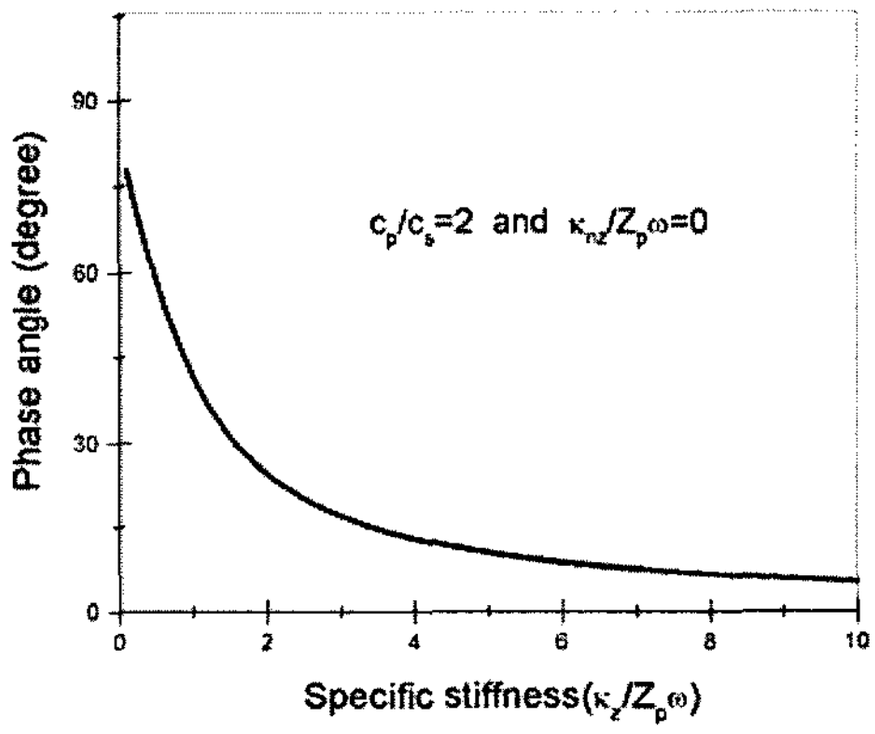

(b) the phase of T

Fig. 5 Transmission coefficient at contact interfaces with respect to the dimensionless specific stiffness $\frac{\kappa_z}{Z_p\omega}$

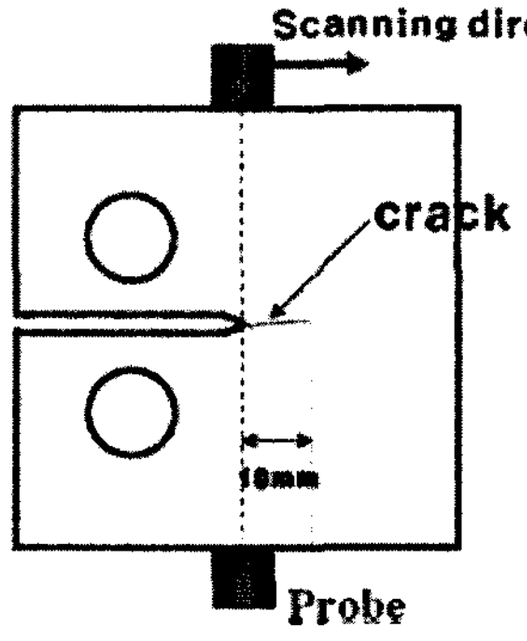

Fig. 6 Fatigue crack in aluminum plate

detected by scanning a transducer of 0.25 inch diameter along the direction of crack propagation in increments of 1mm. The variations of the amplitudes of the reflected and transmitted signals according to the location of the transducer are presented in Fig. 7, where the trian- gular labels represent the reflection signal and the rectangular labels show the amplitude of the transmitted wave. Overall trends of Fig. 7 can be compared qualitatively with the theoretical results shown in Figs. 4 and 5. Even though the horizontal axis in Fig. 7 is different from that of Figs 4 and 5, the scan position in Fig. 7 has a close relation, in qualitative sense, with the specific stiffness in Figs. 4 or 5. As the scan position move away from the notch tip, the crack opening distance(COD) decreases and get closed at a certain distance. The further it is from the notch tip, the higher specific stiffness it has. Therefore it can be assumed that the specific stiffness can be monitored presumably by the scan position. On this assumption, it can be concluded that there exists a good agreement between the experimental and theoretical results in their trends.

The magnitude of the reflection signal has a maximum value near the tip of the notch where the crack is completely open. But it decreases as the measurement position recedes from the notch tip. Beyond 14 mm from the notch tip where the reflection wave disappears, the crack is believed to be closed completely. The reflection wave is still discovered from 10 mm up to 14 mm from the notch tip, which means that the crack propagates about 14 mm from the notch tip even though the crack is not seen beyond 10 mm. In Fig. 7, a maximum reflection does not take place at the tip of the notch, but 3 mm away from the notch. It is mainly because the ultra- sonic wave reflected obliquely and irregularly near the EDM notch tip. It is also partly because of the finite size of the ultrasonic beam which is approximately the transducer diameter 6 mm. It is observed from Fig. 7 that the transmission wave is more sensitive to a closed crack than the reflection wave with a higher signal-to-noise ratio.

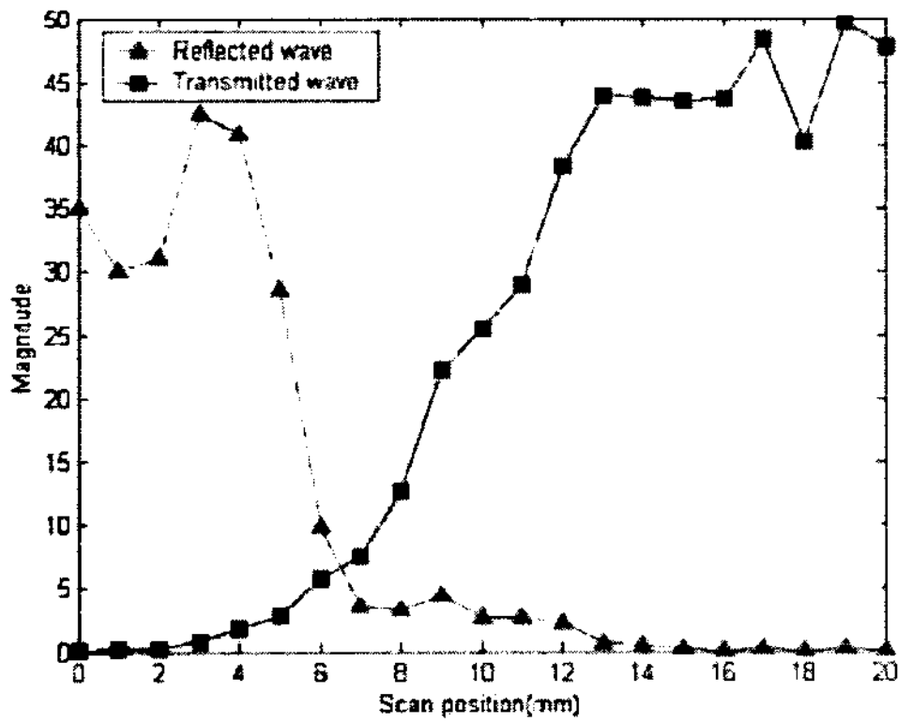

Fig. 7 Variations of reflection and transmission waves in amplitude

6. Conclusions

A hysteretic acoustic nonlinearity model of contact interfaces was developed using Coulomb damping to investigate the characteristics of the reflection and transmission coefficients for a harmonic incident wave at contact interfaces. Based on the hysteretic interfacial stiffness of the contact interface, the tractions on both sides of the interface were defined in terms of the discontinuous displacements across the interface to derive the differential equation for reflected and transmitted waves. Analytic harmonic solutions were obtained to do a parametric study for the reflection and transmission coefficients. It was found from the study that the amplitudes of the reflected and transmitted waves were highly dependent on the frequency and the hysteretic stiffness. As the frequency of the incident wave increased, the higher reflection and lower transmission were obtained. The study also showed that the hysteresis of the interface increased the reflection coefficient, while it reduced the transmission coefficient. For the demonstration of these characteristics of the hysteretic model, a fatigue crack was made in aluminum specimen and examined by pulse-echo and through-transmission tests to measure the

reflected and transmitted waves at different locations of the crack. A stronger reflection was obtained where the crack COD was relatively larger depending on the distance from the notch tip. On the contrary, the transmitted waves became stronger when the COD was smaller or the crack closed. It was concluded that the model developed in this paper agrees with the experimental results in qualitative sense, and might serves as a tool for the characterization of the reflection and transmission at nonlinear contact interfaces.

Acknowledgments

This work was supported by the Korea Science and Engineering Foundation (KOSEF) grant funded by the Korea government (MOST).

References

Aleshin, V. and Van Den Abeele, K. (2007) Micro-Contact Based Theory for Acoustics in Micro-Damaged Materials, Journal of the Mechanics and Physics of Solids, Vol. 55, pp. 366–390

Biwa, S., Suzuki, A. and Ohno, N. (2005) Evaluation of Interface Wave Velocity, Reflection Coefficients and Interfacial Stiffnesses of Contacting Surfaces, Ultrasonics, Vol. 43, pp. 495–502

Biwa, S., Hiraiwa, S. and Matsumoto, E. (2006) Experimental and Theoretical Study of Harmonic Generation at Contacting Interface, Ultrasonics, Vol. 44, pp. 1319–1322

Biwa, S., Hiraiwa, S. and Matsumoto, E. (2007) Stiffness Evaluation of Contacting Surfaces by Bulk and Interface Waves, Ultrasonics, Vol. 47, pp. 123–129

Delsanto, P. P., Hirsekorn, S., Loparco, V. A. and Koka, A. (2002) Modeling the Propagation of Ultrasonic Waves in the Interface Region between two Bonded Elements, Ultrasonics, Vol. 40, pp. 605–610

Kim, J. Y., Baltazar, A. and Rokhlin, S. I. (2004) Ultrasonic Assessment of Rough Surface Contact between Solids from Elasto-Plastic Loading-Unloading Hysteresis Cycle, Journal of the Mechanics and Physics of Solids, Vol. 52, pp. 1911-1934

Kim, J. Y., Baltazar, A. J., Hu, W. and Rokhlin, S. I. (2006) Hysteretic Linear and Nonlinear Acoustic Responses from Pressed Interfaces, International Journal of Solids and Structures, Vol. 43, pp. 6436–6452

Kim, N. and Yang, S. (2007) Nonlinear Displacement Discontinuity Model for Generalized Rayleigh Wave in Contact Interface, Journal of the Korean Society for Nondestructive Testing, Vol. 27, No. 6, pp. 582-590

Nazarov, V. E., Radostin, A. V., Ostrovsky, L. A. and Soustova, I. A. (2003) Wave Processes in Media with Hysteretic Nonlinearity. Part I, Acoust. Phys., Vol. 49, No. 3, pp. 344–353

Pyrak-Nolte, L. J., Myer, L. R. and Cook, N. G. W. (1990) Transmission of Seismic Waves Across Single Natural Fractures, J. of Geo. Res., Vol. 95, No. B6, pp. 8617-8638

Solodov, I. Y. (1998) Ultrasonics of Non-Linear Contacts: Propagation, Reflection, and NDE Applications, Ultrasonics, Vol. 36, pp. 383-390

Zumpano, G. and Meo, M. (2007) A New Nonlinear Elastic Time Reversal Acoustic Method for the Identification and Localisation of Stress Corrosion Cracking in Welded Plate-Like Structures – A Simulation Study, International Journal of Solids and Structures, Vol. 44, pp. 3666–3684